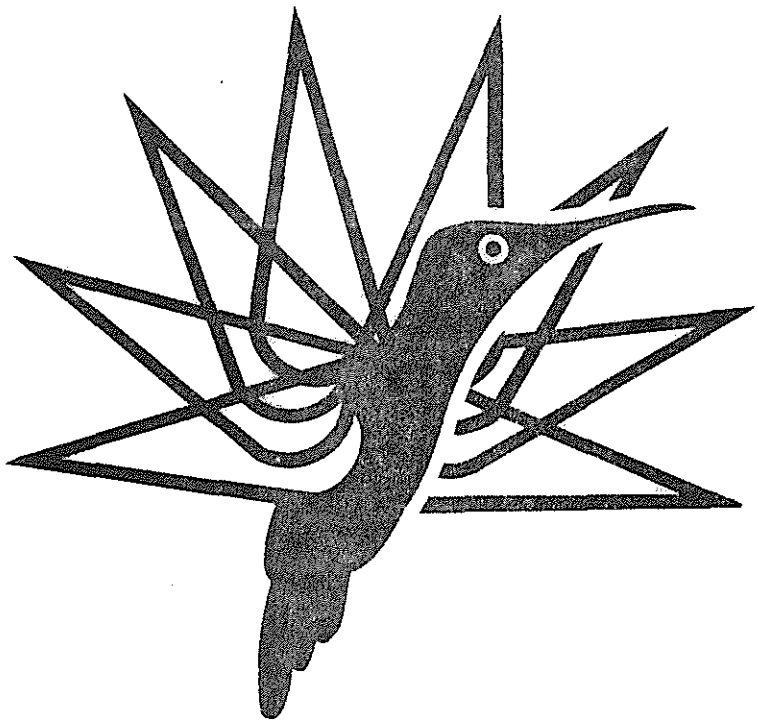

UNSTEADY AERODYNAMICS OF AN AEROFOIL AT HIGH ANGLE OF INCIDENCE PERFORMING VARIOUS LINEAR OSCILLATIONS IN A UNIFORM STREAM

by

C. MARESCA ; D. FAVIER ; J. REBONT

Institut de Mécanique des Fluides

Université d'Aix-Marseille II

France

FIFTH EUROPEAN ROTORCRAFT AND POWERED LIFT AIRCRAFT FORUM

SEPTEMBER 4 – 7TH 1979 - AMSTERDAM, THE NETHERLANDS

UNSTEADY AERODYNAMICS OF AN AEROFOIL AT HIGH ANGLE OF INCIDENCE PERFORMING VARIOUS LINEAR OSCILLATIONS IN A UNIFORM STREAM

C. MARESCA ; D. FAVIER ; J. REBONT
Institut de Mécanique des Fluides
Université d'Aix-Marseille II

ABSTRACT

In forward flight of helicopter, the flow past the blades remains complex owing to 3-D and unsteadiness. One can try to model such a flowfield by unsteady 2-D experiments. Most of the experimental and theoretical studies undertaken on this topic have tackled the problem by investigating aerofoils oscillating in pitch in steady flow, while little attention has been paid to the simultaneous effect of oscillating velocity and oscillating incidence on stalled regions. The aim of this paper is to present a new approach of the experimental study of a stalled rotor blade by investigating the flowfield around an aerofoil performing linear oscillations in a uniform stream. In particular, the case of an oscillation of oblique direction with respect to the undisturbed flow involving simultaneously incidence and velocity out of phase variations is studied.

Aerodynamic forces and skin friction measurements have shown that the aerofoil experiences dynamic stall and dynamic reattachment, characterised by strong unsteady effects leading to an overshoot of the instantaneous lift and drag. Favourable effects on the mean lift coefficient have been pointed out.

NOTATIONS — Unit

A : Amplitude of the oscillation — m

$A_{(i)}$; $B_{(i)}$; $C_{(\varepsilon)}$: see eq. 2

c : chord of the profile — m

C_n : coefficient of Fourier analysis as defined by eq. 1

D : drag — N

f : frequency of the oscillation — Hz

i : unsteady aerofoil incidence — °

i_{ss} : incidence of static stall

$k = \frac{c\omega}{2V_\infty}$: reduced frequency

L : lift — N

$Re_c = \frac{V_\infty . c}{\nu}$: Reynolds number

t : time — s

V : unsteady velocity — $m.s^{-1}$

V_∞ : velocity of the undisturbed upstream — "

α_o : steady aerofoil incidence — °

δ : angle of the oblique direction of oscillation with V_∞ — °

$\varepsilon = \frac{\lambda}{k}$

$\lambda = \frac{A\omega}{V_\infty}$: reduced amplitude

ω : rotational frequency — $rad.s^{-1}$

τ : skin friction — $N.m^{-2}$

ϕ : phase of Fourier analysis as defined by eq. 1

I. INTRODUCTION

Unsteady flows over lifting surfaces occur in a wide range of aerodynamic problems encountered in nature (birds and insects flights) and in actual technique of turbomachines and helicopter rotors for instance, which have received an upsurge of research activity in recent past years. Due to 3-D and unsteadiness, the flow past the rotor of a helicopter in forward flight remains very complex. Relative to the individual blade elements, the surrounding airstream changes periodically with large amplitude fluctuations of velocity magnitude and chordwise incidence. It has been suggested [1] that the crossflow velocity component and the centrifugal effects due to blade rotation can be neglected as far as unsteady stalling features are concerned. The basic features of such an unsteady flow can fundamentally be studied through 2-D models executing cyclic time dependent motion, i.e. the complex aerodynamic behaviour of a blade section away from the tips can be modelled by the simplified case of a 2-D aerofoil oscillating in pitch in an airstream of sinusoïdally varying velocity. Very few experimentalists have paid attention to the effects of oscillating airstreams over pitching aerofoils [2] [3] when most of the theoretical and experimental works in the field have been devoted to the case of an aerofoil oscillating in pitch around a mean incidence in a steady 2-D airstream. Special considerations have been given to the so-called "dynamic stall" occurring when the aerofoil operates at incidences higher than the static stall incidence. A recent paper [4] summarizes some of the major investigations undertaken on this topic.

A new approach to rotor blade stall analysis has been attempted at the Institute of Fluid Mechanics of Marseille to model the unsteady events [5] occurring on rotor blade in forward flight, by achieving other types of time dependent motion. Harmonic motion of an aerofoil at fixed incidence oscillating in translation parallel (fore and aft motion), normal (plunging motion) or oblique to an undisturbed flow, are studied.

The first kind of motion simulates the variations of velocity, the second one the variations of incidences and the third one the variations out of phase of both velocity and incidence.

The experiments performed in a subsonic wind tunnel are presented for static incidences of the oscillating aerofoil (a NACA 0012) larger than the incidence for maximum static lift. The investigations have been carried out by means of several measuring techniques suitable for unsteady flow analysis : torsion dynamometers, pressure transducers and skin friction gauges at the surface of the aerofoil.

The results show that in all cases of motion, dynamic stall and dynamic reattachment contribute to a favorable effect of unsteadiness on the mean lift coefficient which increases as compared to the steady state one.

2. EXPERIMENTAL FACILITIES

The tests were conducted in the IMFM low turbulence open circuit wind-tunnel (test section of 0.5 x 1 x 3m). Upstream of the nozzle seven high solidity screens reduce the free stream turbulence level to 0.2 %. The test section velocity, under steady flow conditions can be varied from 2.5 to 20 m/s. The model is a rectangular wing (span $l = 0.495$ m and chord $c = 0.3$ m) with a NACA 0012 profile. The static stall angle of incidence is 12° and the range of Reynolds number is $5.7\ 10^4 \leq Re_c \leq 4 \times 10^5$.

The wing which spans the entire test section, is held vertically by two inside masts passing through a gap on the bottom of the test section. These masts are supported by a suspension gear fixed on a frame oscillating sinusoidally in translation. The wing excepted, the experimental set up is located on the outside of the test section. The direction of the translation can be set parallel, normal or oblique to the stream of the wind tunnel.

The wing can move freely in the test section as its span (0.495 m) is slightly smaller than the test section height (0.5 m). As the aspect ratio of the wing is about 8, no steady correction of end effects was done. The

static pressure along the wall of the test section is very nearly equal to the outside atmospheric pressure, so that there is no flow through the gap provided on the wall to support the instrumented aerofoil.

The aerodynamic forces (lift and drag) and the aerodynamic moment at the quarter chord point of the aerofoil were measured by help of torsion dynamometers dynamically calibrated and described in ref. (5).

Local static pressures were measured at the surface of the aerofoil by ten "kulite" pressure transducers (CQH125). Local skin friction measurements were performed by means of nine hot-film gauges mounted flush with the aerofoil surface. The unsteady values of the skin friction were non-dimensionalized by the correlated steady values so that no quantitative calibration was required to evaluate the unsteadiness, assuming that the steady flow calibration was still valid in periodic flow ; the movement frequency (<5 Hz) is low compared to the high frequency response of the gauge (≃ 10^6 Hz).

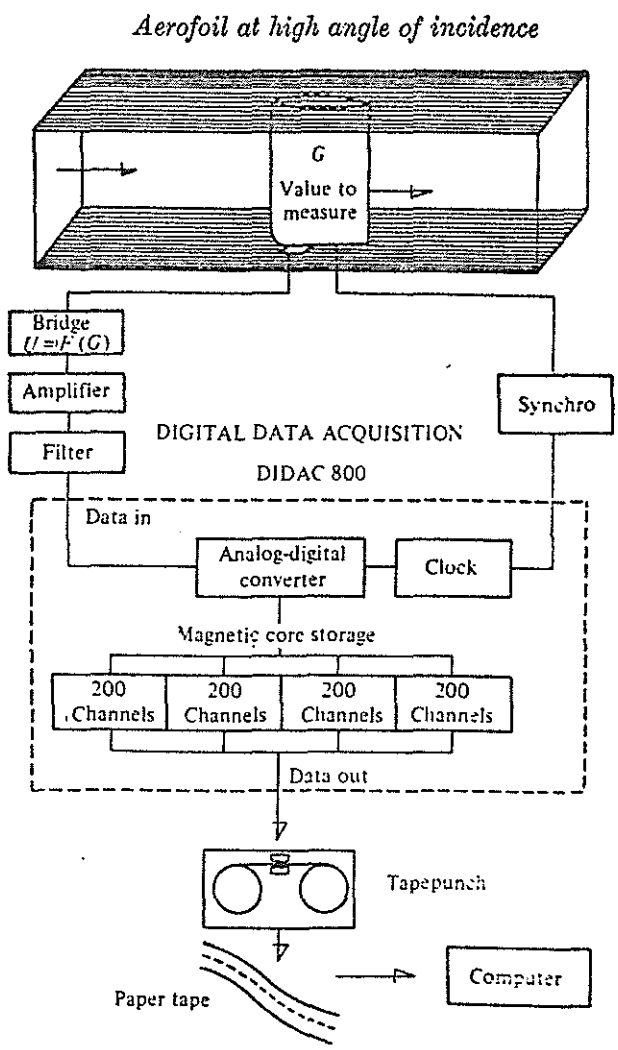

FIGURE 1. Block diagram of data acquisition.

As shown on the figure [1], the measurements of forces, pitching moment, static pressure and skin friction were digitized and stored by a 800-channel data acquisition system (Intertechnic DIDAC 800). The time history of the quantity G to be measured was performed at 200 different phases of a single period and stored on 20 cycles of oscillations. The data were then harmonically analysed in N Fourier harmonics in the following form :

$$G/G_s = C_o + \sum_{n=1}^{n} C_n \cos(n\omega t + \phi_n) \qquad (1)$$

where G_s is the static value and C_o the time averaged value of G/G_s over a period.

3. TEST CONDITIONS

The test conditions are listed in the following table and are relative to the three kinds of unsteady motion

Table 1

	From	to	Notations
Airstream velocity (m/s)	2·5	20	V_∞
Aerofoil incidence (deg)	$-25°$	25°	i
Oscillating amplitude (m)	0	0·17	A
Oscillating frequency (Hz)	0	5	f
Reynolds number/chord	$5{\cdot}7 \times 10^4$	4×10^5	Re_c
Reduced amplitude	0	1·20	λ
Reduced frequency	0	1·60	k
Ratio $\epsilon = \lambda/k = 2\,(A/c)$	0	1·13	ϵ

4. RESULTS

4.1. Fore and aft motion : This oscillation has been extensively studied at the IMFM and the following results are described in details in Ref. (6). Such a kind of motion, figure [2], leads to a relative velocity of the model given by the equation $v/v_\infty = 1 + \lambda \cos\omega t$. The incidence is constant along the period and equal to α_0.

TRANSLATORY UNSTEADY MOTIONS OF AIRFOIL IN 2D STEADY FLOW

$$\lambda = \frac{A\omega}{V_\infty} \quad ; \quad K = \frac{c\omega}{2V_\infty}$$

I. FORE AND AFT MOTION

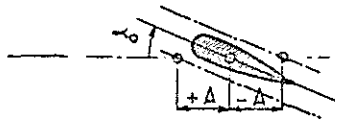

Incidence: $i = \alpha_0 = C^{te}$

Velocity : $V = V_\infty (1 + \lambda \cos \omega t)$

II. PLUNGING MOTION

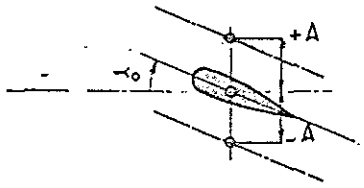

Incidence: $i = \alpha_0 + \text{Arc tg.}\,(\lambda \cos.\omega t)$

Velocity : $V = V_\infty \sqrt{1 + \lambda^2 \cos^2 \omega t}$

Figure 2.

III. OBLIQUE MOTION

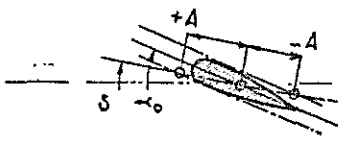

Incidence: $i = \alpha_0 - \text{Arc tg.}\left[\frac{\lambda \cos.\omega t \sin\delta}{1 + \cos \omega t \cos\delta}\right]$

Velocity : $V = V_\infty \sqrt{(1 + 2\lambda \cos\omega t \cos\delta + \lambda^2 \cos^2 \omega t)}$

The results concerning the time averaged overall forces and moment deduced from the torsion dynamometers measurements have clearly demonstrated that the unsteady effects are weak at incidences below the angle of static stall i_{ss} but get rapidly significant when λ and k increase for incidence above i_{ss} [6].

The mean lift-steady lift ratio C_o as defined by G/G_s and obtained for the test conditions of Table 1 has been synthetized by the following empirical formula :

$$C_o = 1 + A(i)\ \varepsilon^{\alpha}\ k^2\ [1 - B(i)k(\varepsilon)^{C(\varepsilon)}], \qquad (2)$$

where : if $i \leq i_{ss}$ $A(i) = 0.782\ (\frac{i}{i_{ss}})$; $\alpha = 4$; $B(i) = 0.2$; $C(\varepsilon) = 5$

$$\text{if } i \geq i_{ss} \begin{cases} A(i) = 4 + 0.6\ (\frac{i}{i_{ss}}) \ ; \ \alpha = 1, \\ B(i) = 0.558 + 0.432\ \left| 2.17 - (\frac{i}{i_{ss}}) \right|^3 ; \\ C(\varepsilon) = 0.422 - 055\varepsilon. \end{cases}$$

As an example, figure [3] shows for $i = 20°$, the experimental values of C_o versus k for several values of ε.

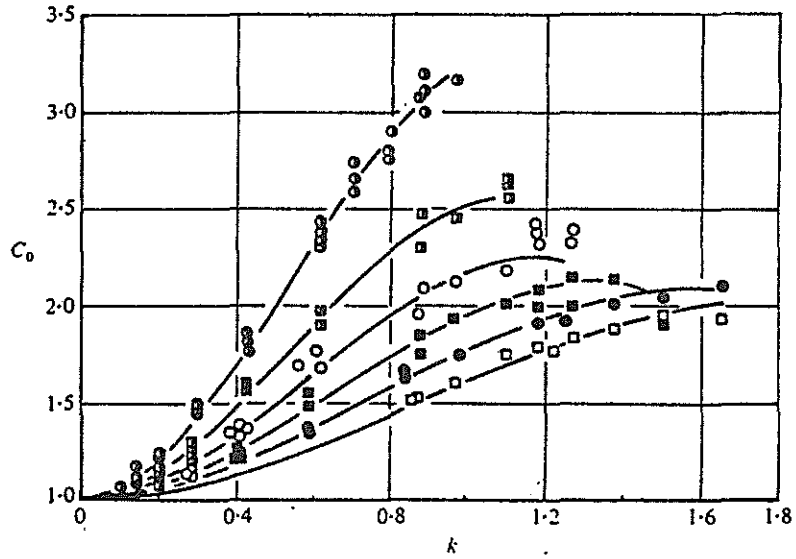

Dash lines represent equation (2). The gathering of data obtained at fixed ε and k for several V_∞ and ω shows that the parameter k keeps a universal character at least in the range $5.710^4 \leq Re_c \leq 4.10^5$.

FIGURE 3. Variation with k of C_0 = (averaged lift $\bar{L}$)/(steady lift L_s) $i = 20°$; $0{\cdot}715 \times 10^5 < Re_c < 4{\cdot}10^5$. ——, equation (1). Experiments, ε values: ◑, 1·13; ▨, 0·79; ⊙, 0·55; ■, 0·39; ●, 0·27; □, 0·19.

The unsteady effects produced by the fore and aft motion of the wing induce an overshoot of the mean lift coefficient. This lift coefficient gain is however coupled with a drag and moment coefficients increase (These results are given in ref. 6). At angles of attack above i_{ss}, the dynamic data indicate averaged wake width and nose-down moments larger than the steady ones, as λ increases from 0 to 0.74.

The increase of the mean lift compared to the static value is confirmed by pressure measurements performed on the model. The mean lift calculated by integration of the mean pressure coefficient plot on the figure [4] for $i = 20°$, $\lambda = 0.744$ and $k = 0.657$ would be about 2.1 times higher than the mean lift given by the static pressure coefficient data plot on the same figure. This value is in good agreement with the result of torsion dynamometer.

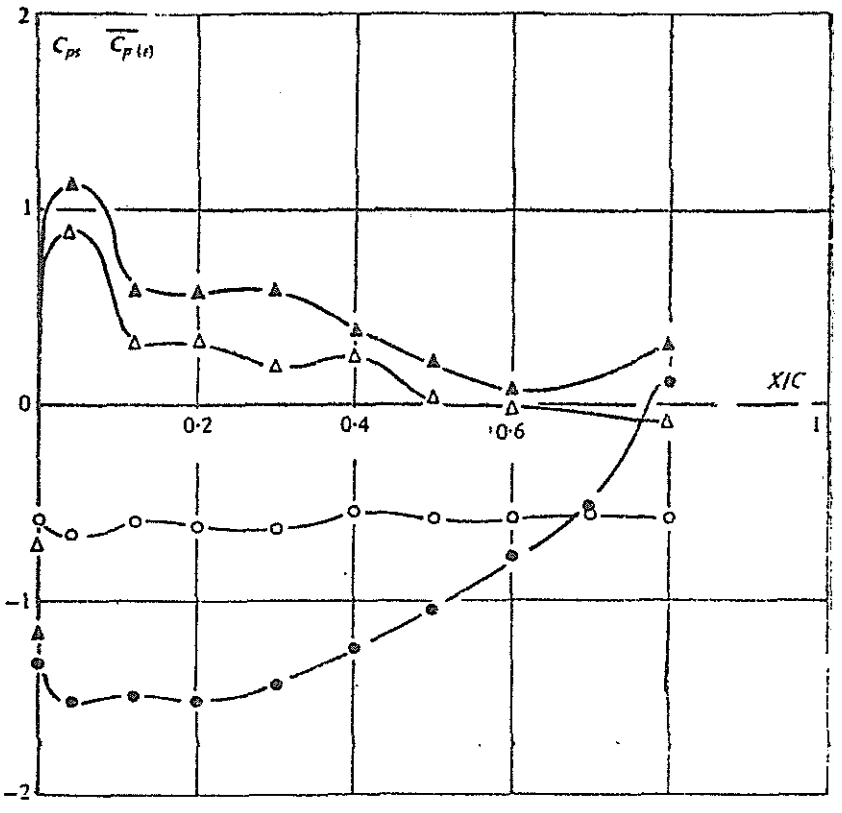

FIGURE 4. Distribution of averaged $\overline{C_{p(t)}}$ and steady C_{ps} pressure coefficient. $i = 20°$; $A = 0{\cdot}17$ m; $f = 2{\cdot}5$ Hz; $A/c = 0{\cdot}565$; $\epsilon = 1{\cdot}13$; $Re_c = 0{\cdot}714 \times 10^5$; $\lambda = 0{\cdot}744$; $k = 0{\cdot}657$. Upper surface: ○, steady; ●, average value. Lower surface: △, steady; ▲, average value.

The results concerning visualization and instantaneous measurements[6] have shown that aerofoil in fore and aft motion was experiencing both dynamic stall and dynamic reattachment. Dynamic stall is initiated by a large bubble which bursts giving rise to vortex shedding characterised by a vortex rolling from the leading edge to the trailing edge. This vortex shedding process induces instantaneous lift and drag overshoots and maximum diving moment. The dynamic reattachment which occurs progressively from the leading edge may be observed at very high incidence (20°) for a short part of the period when the aerofoil is moving forward in accelerated motion.

4.2. Plunging motion : The static angle of attack is set at α_o and the aerofoil is put in oscillation in a direction normal to the undisturbed upstream, as shown on figure 2. The instantaneous incidence and velocity are given by :

$$i = \alpha_o + \text{Arc tg}\,(\lambda \cos \omega t)$$

$$V = V_\infty \sqrt{1 + \lambda^2 \cos^2 \omega t}$$

In the case of small values of λ, the above equation can be linearised as follows :

$$i = \alpha_\Theta + \lambda \cos \omega t + O(\lambda^2) \qquad (3)$$

$$V = V_\infty + O(\lambda^2) \qquad (4)$$

The unsteady effects induced by the variations of i have already been studied (see ref (7) for instance) from experiments realised in wind tunnel on pitching aerofoils. The results show the existence of hysteresis loops appearing on lift and moment when the incidence is varying periodically from low values to values sufficiently high to generate dynamic stall.

It is interesting to compare the results obtained in pitching motion to those obtained in plunging motion as the variation of incidence and velocity are given by the same equations (3) and (4) in both cases. For a corect comparison, the virtual mass experienced in plunging motion can be neglected as it is the case in pitching motion. This assumption is valid as long as λ and k remain low.

Figure [5] presents for $\lambda = 0.177$ and $k = 0.156$ the loop of hysteresis obtained on lift coefficient in plunging motion (full line) and in pitching motion (dash line). In both cases k is equal to 0.15, the mean angle of incidence is 15° and the magnitude of incidence oscillation is $\Delta i = 10°$.

Figure 5

LIFT VARIATIONS WITH INCIDENCE IN PITCHING AND PLUNGING MOTIONS

—— PLUNGING MOTION
$k=0.15$; $\alpha_o = 15°$; $\Delta i = \pm 10°$; $Re_c = 2.4.10^5$

---- PITCHING MOTION [7]
$k=0.15$; $\alpha_o = 15°$; $\Delta i = \pm 10°$; $Re_c = 2.5.10^6$

●●●●● STEADY FLOW

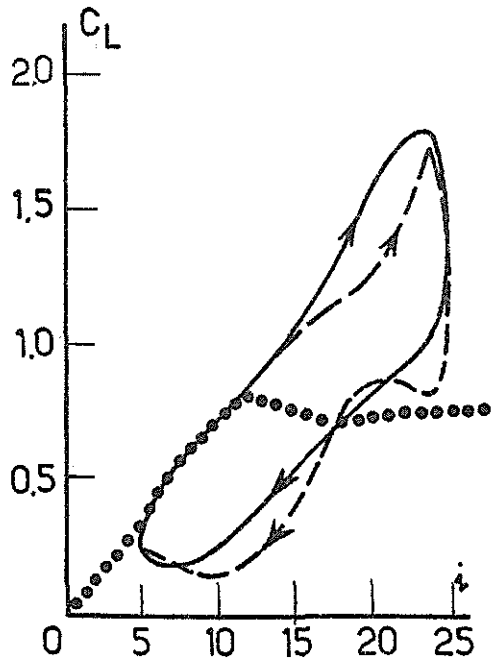

Reynolds number are different : $2.4.10^5$ for plunging motion and $2.5.10^6$ in pitching motion. It can be seen that for these low values of λ and k the variations of lift relative to the two different motions are in good agreement. The lift has been measured by torsion dynamometer for the present experiments and by integration of a wall pressure distribution for pitching motion [7]. The variation of steady lift with incidence has also been represented on the figure by a dotted line in order to appreciate the unsteady effects. As it has already been observed in pitching motion, the visualisations performed in plunging motion show clearly that the boundary layer remains attached at incidence as high as 20°. Moreover, when the incidence is decreasing, it can be observed that the flow is separated at very low incidence (6°) as indicated by the low value of the lift on figure [5].

Figure [6] shows the drag variation with incidence obtained in plunging motion by torsion dynamometer measurements. In the region of low angles of incidence the unsteady drag is close to the steady values and exhibits two loops of hysteresis. It has not been possible to compare plunging to

pitching drag measurements because, to our knowledge, no direct drag measurements in this last case are available in the literature. Concerning the moment coefficient, the comparison has been realised as is shown on figure [7].

In the region of high angles of attack, a large loop of hyteresis in drag and two loops in moment are pointed out. It can be seen that the maximum of drag (fig. [6]) corresponds to the maximum of lift (fig.[5]). When the moment stall occurs (fig. [7], i ≃ 15°) the drag increases sharply (i ≃ 15°). It is interesting to note that the lift stall beings later (i ≃ 23°). These events corroborate the well-known vortex shedding phenomenology given in the literature and concerning dynamic stall on pitching aerofoils.

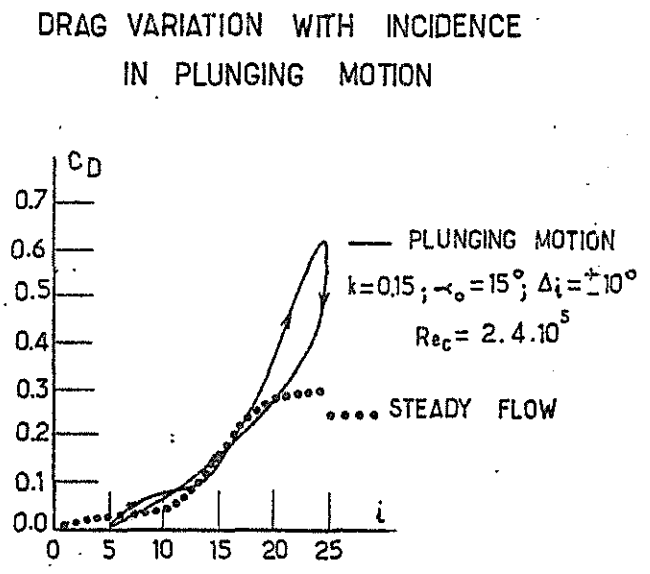

Figure 6

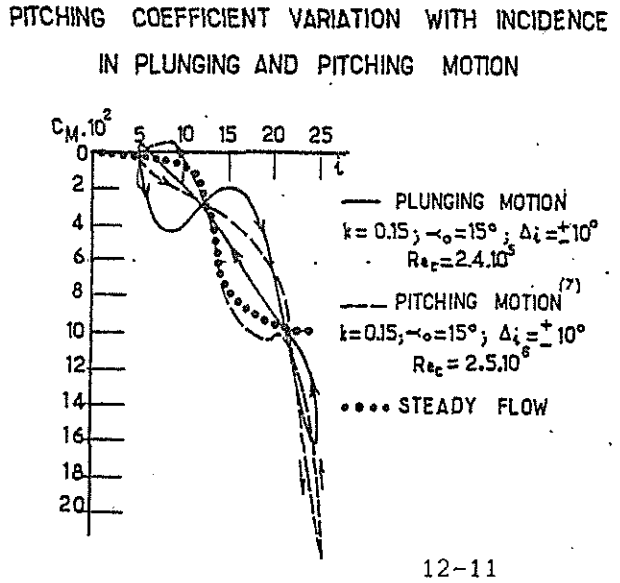

Figure 7

4.3. Oblique motion

As exemplified on the diagram of figure[2] the static angle of attack α_o can be set up anywhere between -25° and 25° ; the aerofoil is then put in oscillating translation along the X_δ oscillation axis. The angle δ between the X_δ axis and the airstream direction can be adjusted from 0° to 90° ; when δ = 0° or 90° the aerofoil oscillates respectively in fore and aft motion or in plunging motion.

The incidence i between the resultant velocity V and the chord is given by :

$$i = \alpha_o - i_o \quad \text{with} \quad i_o = \text{Arc tg} \left(\frac{\lambda \cos\omega t}{1+\cos \omega t \cos\delta} \sin\delta \right) \qquad (5)$$

The velocity V is given as follows :

$$V = V_\infty \sqrt{1+ (2 \lambda\cos\delta\cdot) \cos \omega t + \lambda^2\cos^2 \omega t} \qquad (6)$$

Figure 8

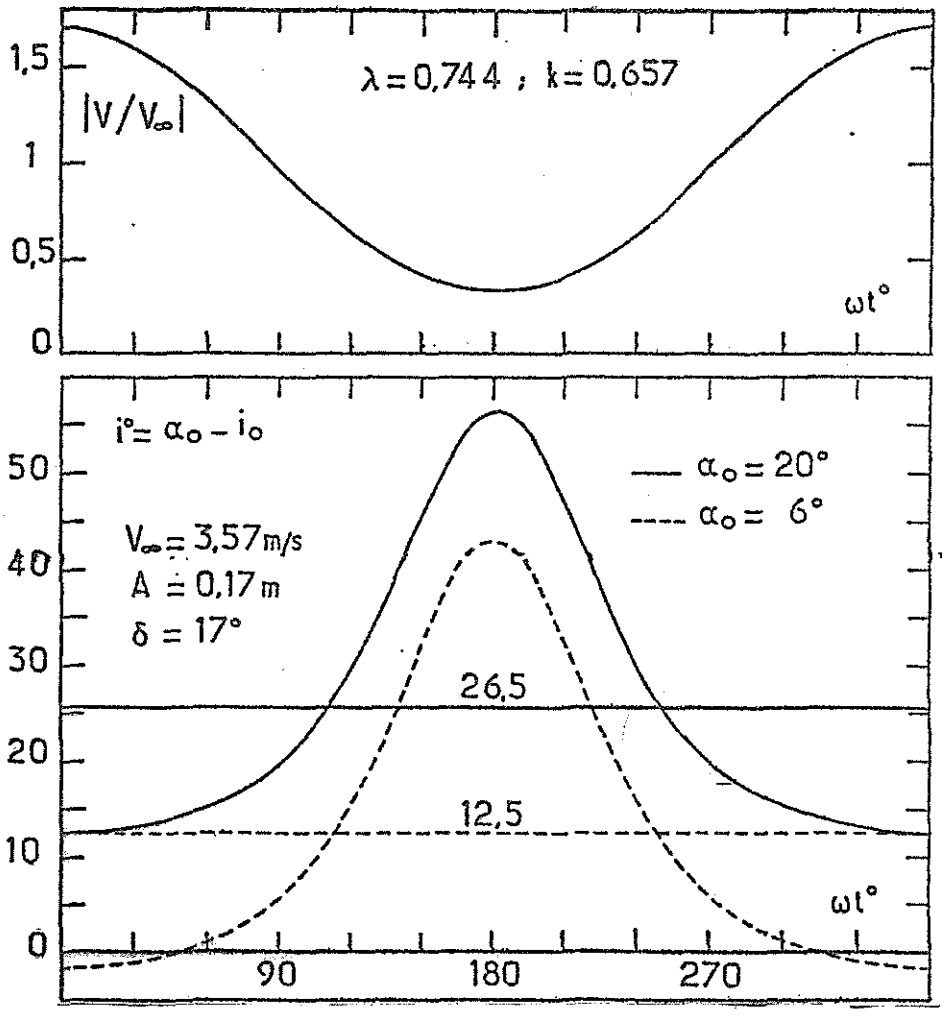

So, large amplitude variations out of phase of both velocity and incidence can be obtained (the maximum velocity coinciding with the minimum incidence).

Figure [8] represents the periodic variations of V and i versus ωt, for two values of α_o= 20° and 6°, in the following conditions : δ = 17° λ = 0.744 ; k = 0.66. As an example, it can be seen that for α_o= 20°, i can reach very high instantaneous values ranging from 57° to 12.8° around a mean incidence of 26.5°. In this case, the magnitude of the velocity variation ΔV is large too : $\frac{\Delta V}{\overline{V}} \simeq 0.74$.

Figures [9] and [10] show the evolutions of instantaneous lift and drag for V_∞ = 3.5 m/s ; δ = 17° ; λ = 0.744 ; k = 0.657 , when α_o = 20°. Quasi steady variations of lift and drag (L_{QS} and D_{QS}) which should be obtained when the aerofoil behaviour remains quasi-steady are also shown on the figures in order to underline truly unsteady effects.

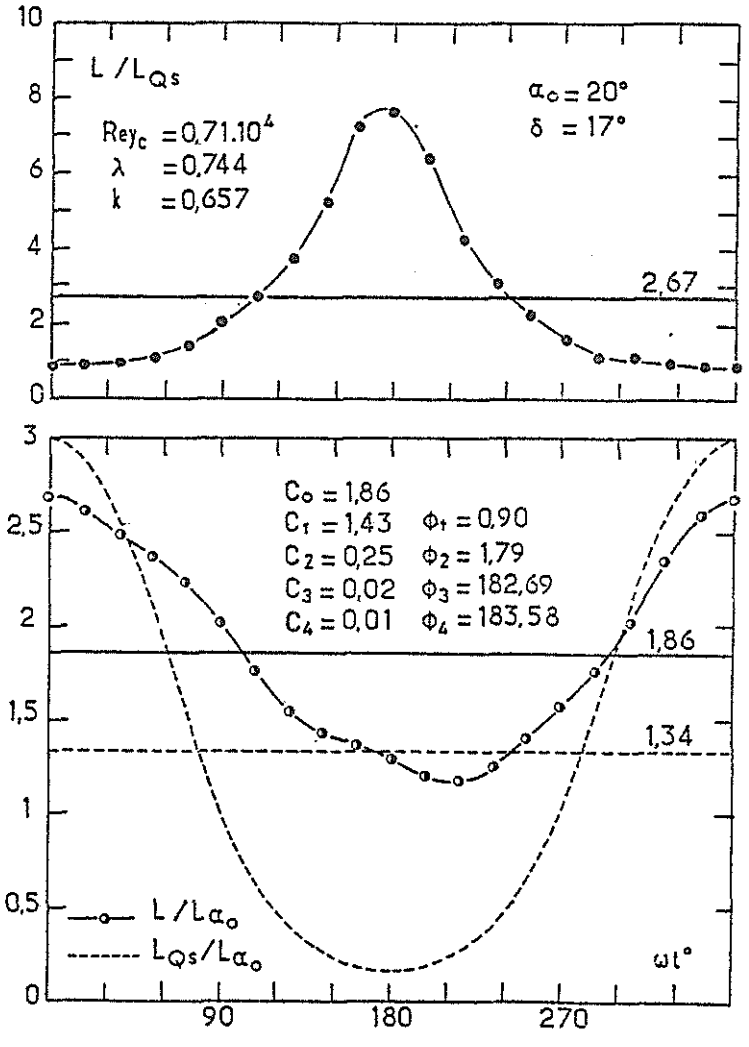

Figure 9

L_{QS} and D_{QS} (dotted lines) have been calculated from the steady values of L and D (see ref.(6)) when V and i are varying with time according to equations (5) and (6). For incidences above 25° (which is the experimental limit for the measurement of L in ref.(6)), it has been assumed that the stalled aerofoil has a steady aerodynamic behaviour similar to a flat plate set at incidence i in an air-stream of speed V. L, D, L_{QS} D_{QS} have been normalised by the steady lift and drag ($L_{\alpha o}$ and $D_{\alpha o}$) measured at α_o = 20° and V_∞ = 3.57 m/s. The time histories of L and D represented on figures [9] and [10] by dash lines correspond to the Fourier 4 harmonic analysis of experimental results according to equation of G/G_s, (equ. 1) . The instantaneous lift L (figure [9]) which remains above the steady lift $L_{\alpha o}$ over the whole period exhibits significant increases. Its time averaged value (C_o = 1.86) is also greater than the

quasi steady one (1.34). An overshoot of the instantaneous drag D is readily observable on figure [10] where D is equal to the steady $D_{\alpha o}$ for $\omega t \simeq 240°$.

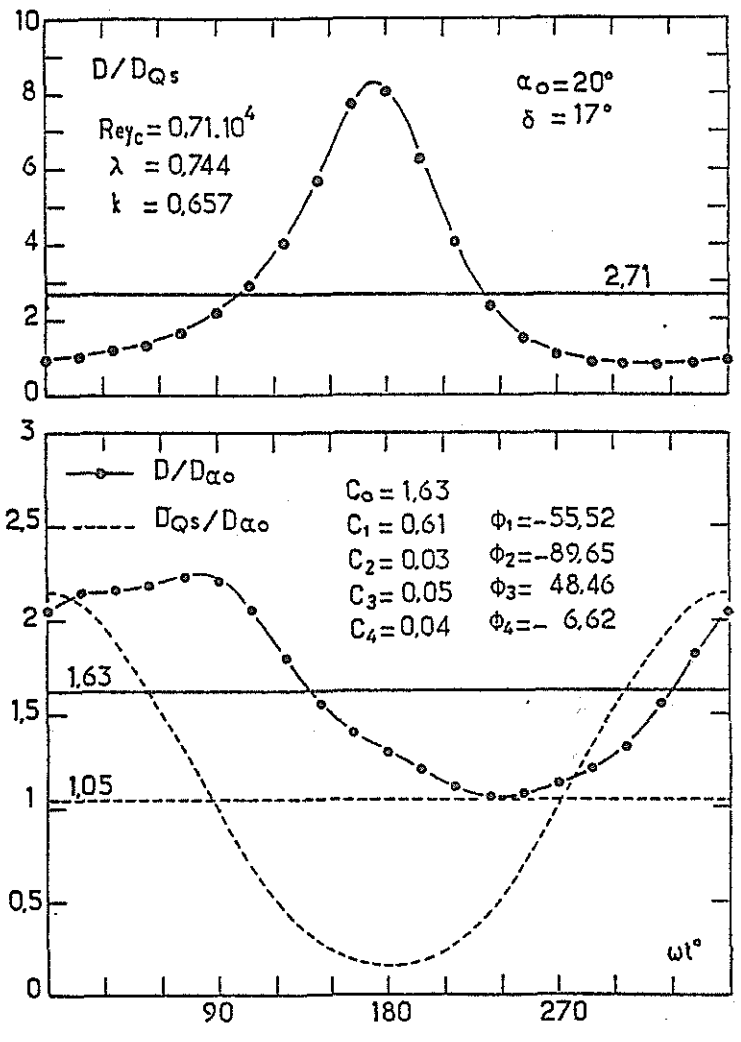

Figure 10

Both $L/L_{\alpha o}$ and $L_{QS}/L_{\alpha o}$ (or $D/D_{\alpha o}$ and $D_{QS}/D_{\alpha o}$) are decreasing as velocity decreases, but it is worth noting that the $L/L_{\alpha o}$ and $D/D_{\alpha o}$ curves are phase lagged and have a nonsymmetrical behaviour for $0 \leq \omega t \leq 180°$ and for $180° \leq \omega t \leq 360°$. The unsteady aerodynamic load is higher at $\omega t = 90°$ for decreasing velocity than at $\omega t = 270°$ when velocity is increasing ; nevertheless, for both phases 90° and 270° V and i have the same value ($V = V_\infty$, $i = \alpha o = 20°$).

Data of L/L_{QS} and D/D_{QS} plotted versus ωt on tops of fig.[9] and [10] clearly demonstrate the significant deviation from the expected quasi-steady behaviour. Indeed the time-averaged value is of about 2.7 for lift and drag, and when $\omega t \simeq 180°$ (which is the maximum incidence) strongest unsteady effects appear ; L and D are then respectively equal to 7 L_{QS} and 8 D_{QS}.

Moreover, it has been possible to plot on figure [11] the time history of skin friction τ / τ_s from x/c = 0.04 to x/c =0.8, deduced from hot film gauges measurements on the upper side of the aerofoil for $\alpha o = 20°$;

$\delta = 17°$; $\eta = 0.744$ and $k = 0.657$. It can be seen from these waveforms that when fluctuations of incidence and velocity out of phase are realised simultaneously, a rolling vortex phenomenon also appears (as in the "fore and aft" and "plunging" motions) near the leading edge ($x/c = 0.12$) and develops along the aerofoil upper surface. This strong vortex is convected downstream with a speed of propagation of about $0.45\ V_\infty$ and can explain the overshoot of lift drag and pitching moment.

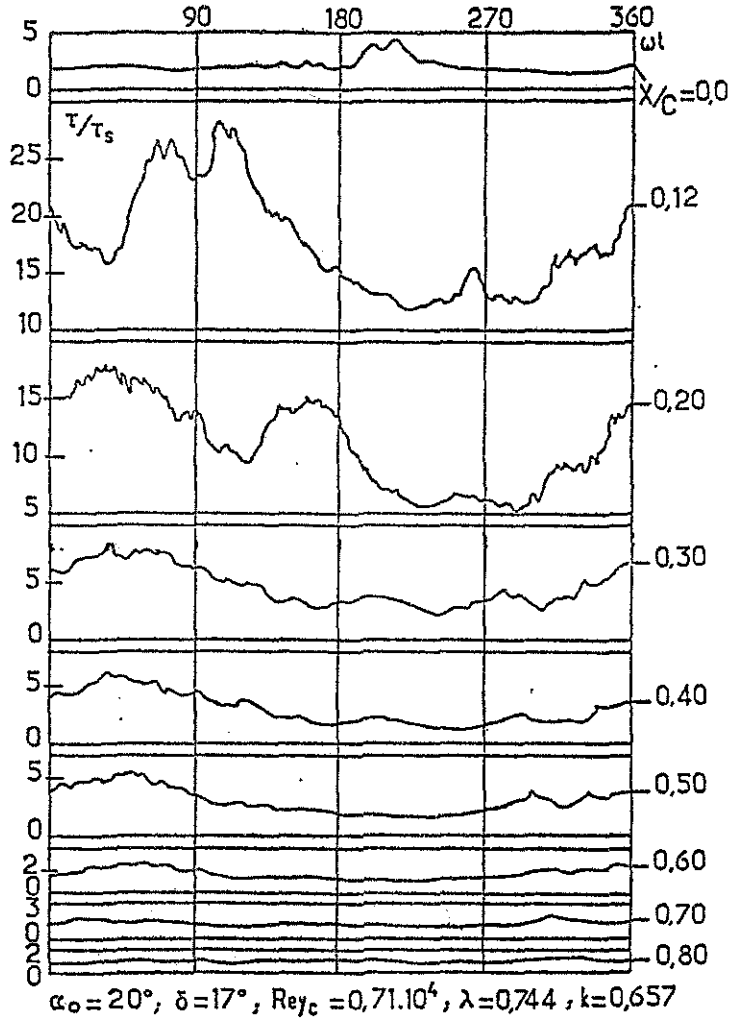

Figure 11

5. CONCLUSIONS

The aim of this set of experimental programmes was to get insight into complex 3-D unsteady flows over advancing or retreating helicopter blade sections. The basic features of such unsteady flows have been pointed out and investigated through two-dimensional models for aerofoils performing various linear oscillations in a uniform airstream. Three kinds of cyclic time dependent motions have been studied in order to simulate simultaneously or separately the variations of incidence and velocity :

. if velocity fluctuations only are concerned (fore and aft motions) unsteady effects are weak as the incidence remains below the angle of static stall. Above the angle of static stall, the effects of unsteadiness are very strong and depend on frequency and amplitude of velocity fluctuations. The mean lift overshoot which could be given by an empirical formula, results from a dynamic stall and reattachment process giving rise to a vortex shedding. The vortex rolling on the upper surface aerofoil also induces a large mean drag and nose down pitching moment. The dynamic reattachment which occurs progressively from the leading edge can be observed at very high incidence for a short part of the period when the aerofoil is going forward in accelerated motion.

. as to the incidence fluctuations (plunging motion) the strongest effects are also obtained for high incidences and for magnitude of incidence oscillations large enough to generate the dynamic stall. In this case the results show the existence of hyteresis loops on lift, drag and moment. The major findings consist in the comparison of the lift and moment loops obtained in plunging motion with those already observed for pitching aerofoils. Unsteady features (on lift moment, pressure and skin friction) are closely similar in both cases. Moreover, all the events of the dynamic stall phenomenology of lift and moment, well known for an aerofoil rotating around its quarter chord point, are well corroborated by the present results when the aerofoil oscillates linearly in plunging motion.

. when large amplitude fluctuations of both velocity and incidence are simulated (oblique motion) all the unsteady features previously mentioned for the simple linear oscillations can be observed and investigated. More particularly, the overshoot of instantaneous lift and drag observed in the present results clearly demonstrate the significant deviation from steady behaviour of the aerofoil. It is hoped that in the future the third kind of motion, which gives a faithful configuration of real rotor blade flows (when neglecting centrifugal effects), will lead to a better understanding of the nature of unsteady effects resulting from velocity fluctuations and those specific of incidence.

REFERENCES

1) W.J. Mc CROSKEY, R.K. FISHER, Detailed aerodynamic measurements on a model rotor in the blade stall regime. J. Amer. Hel. Soc. 17.1.20 - 1972.

2) G.A. PIERCE, J.B. MALONE, The Effect of Varying Freestream Velocity on Dynamic Stall Characteristics, paper presented at the 32nd Annual National AHS Forum, 1976.

3) T. HAJEK, A. FEJER, A new approach to rotor blade stall analysis, paper presented at the 4th European Rotorcraft and Powered Lift Aircraft Forum, 1978.

4) W.J. Mc CROSKEY, Some Current Research in Unsteady Fluid Dynamics. The 1976 Freeman Scholar Lecture. Trans. A.S.M.E. J. Fluid Engng 99, 8, 1977.

5) J. REBONT et al, Recollement dynamique sur un profil d'aile en mouvement de tamis. Influence des paramètres d'oscillation. Presented at the A.G.A.R.D FDP Meeting Unsteady Aerodyn. Ottawa, 1977.

6) C. MARESCA et al, Experiments on an aerofoil at high angle of incidence in longitudinal oscillations. J. Fluid Mech. 92. 24, 1979.

7) L.W. CARR et al, Analysis the development of dynamic stall based on oscillating airfoil experiments. NASA Tech. N.D8382, 1977.